OPEN ACCESS

Microbiology & Biomedicine REPORT

Industrial production of natural low-calorie sweetener neohesperidin dihydrochalcone

Xiaoxi Zhu,[1,2,3,7] Wei Liu,[1,2,6,7] Yuwan Liu,[1,2] Huanyu Chu,[1,2] Jian Cheng,[1,2] Yadi Gao,[4] Jiayu Liu,[1,2] Xiaotong Shao,[1,2,4] Mengheng Xue,[1,2] Nida Ahmed,[1,2] Xiaonan Liu,[5] Lili Song,[4] and Huifeng Jiang[1,2,*]

*Correspondence: jiang_hf@tib.cas.cn

Received: July 15, 2025; Accepted: January 5, 2026; Published Online: January 8, 2026; https://doi.org/10.59717/j.xinn-life.2026.100190

GRAPHICAL ABSTRACT

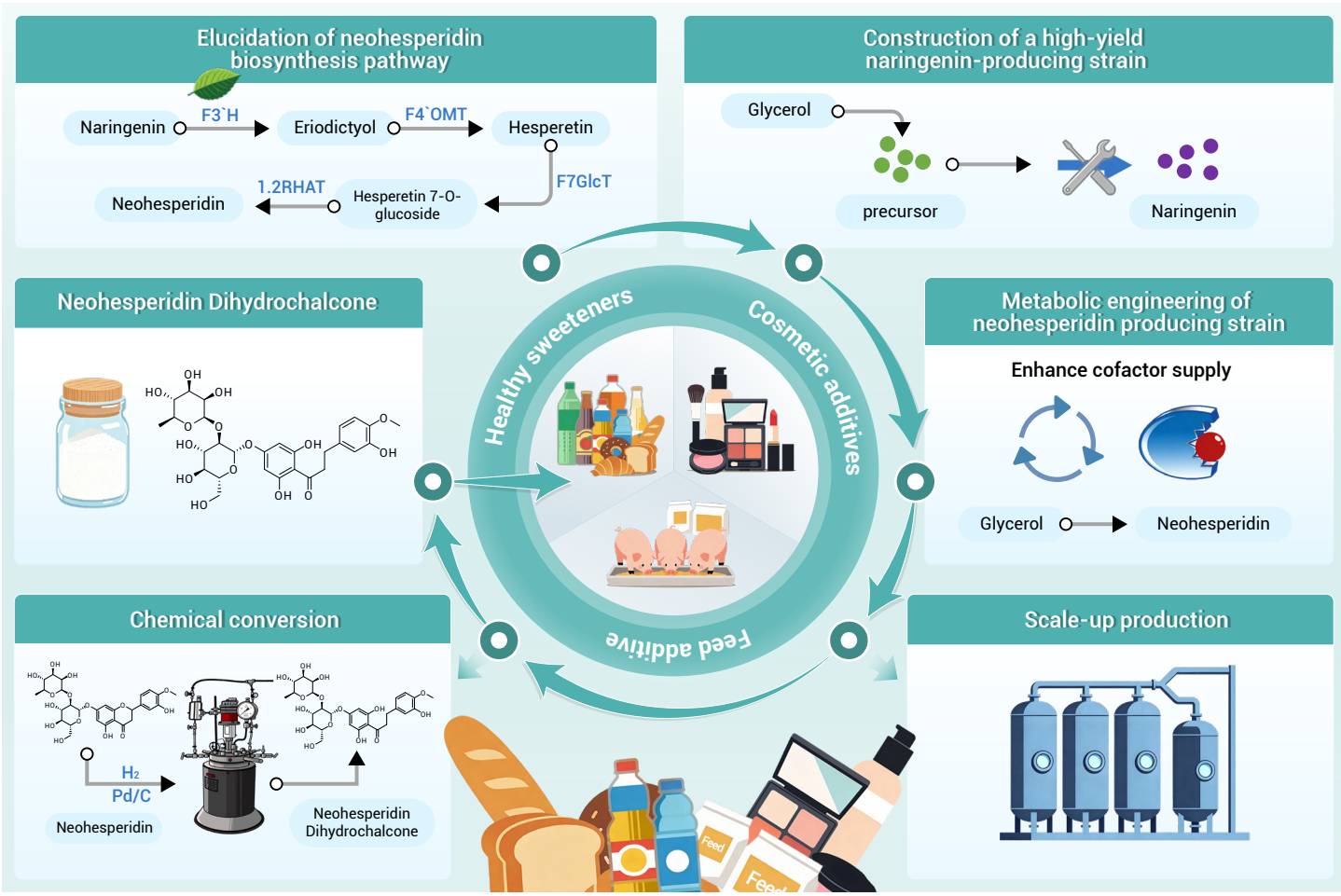

PUBLIC SUMMARY

- Elucidation and construction of neohesperidin biosynthesis pathway in *Yarrowia lipolytica*.
- A biochemical process for producing neohesperidin dihydrochalcone (NHDC) was developed.
- This process enables sustainable, high-yield industrial production of the natural low-calorie sweetener NHDC.

REPORT Microbiology & Biomedicine

OPEN ACCESS

Industrial production of natural low-calorie sweetener neohesperidin dihydrochalcone

Xiaoxi Zhu,[1,2,3,7] Wei Liu,[1,2,6,7] Yuwan Liu,[1,2] Huanyu Chu,[1,2] Jian Cheng,[1,2] Yadi Gao,[4] Jiayu Liu,[1,2] Xiaotong Shao,[1,2,4] Mengheng Xue,[1,2] Nida Ahmed,[1,2] Xiaonan Liu,[5] Lili Song,[4] and Huifeng Jiang[1,2,*]

[1]Key Laboratory of Engineering Biology for Low-carbon Manufacturing, Tianjin Institute of Industrial Biotechnology, CAS, Tianjin 300308, China

[2]National Center of Technology Innovation for Synthetic Biology, Tianjin 300308, China

[3]Anhui Jinhe Industrial Co., Ltd., Chuzhou 239200, China

[4]National Key Laboratory for Development and Utilization of Forest Food Resources, Zhejiang A & F University, Hangzhou 311300, China

[5]College of Bioengineering and Food Science, Hubei University of Technology, Wuhan 430068, China

[6]Medical Engineering & Engineering Medicine Innovation Center, Hangzhou International Innovation Institute, Beihang University, Hangzhou 311115, China

[7]These authors contributed equally

*Correspondence: jiang_hf@tib.cas.cn

Received: July 15, 2025; Accepted: January 5, 2026; Published Online: January 8, 2026; https://doi.org/10.59717/j.xinn-life.2026.100190

Citation: Zhu X., Liu W., Liu Y., et al. (2026). Industrial production of natural low-calorie sweetener neohesperidin dihydrochalcone. *The Innovation Life* **4**:100190.

Neohesperidin dihydrochalcone (NHDC), a natural, low-calorie, high-intensity sweetener derived from plants, faces sustainable supply challenges due to its limited natural abundance. Here we developed a biochemical synthetic process for NHDC production at 5000-L bioreactor system. First, a heterologous synthetic pathway for neohesperidin, which is the precursor of NHDC, was constructed in *Yarrowia lipolytica* through the screening and assembly of candidate genes sourced from 25 species. Through key gene mining, metabolic flux regulation and fermentation optimization, we constructed 106 engineering strains and improved the titers of neohesperidin by 6,481-fold reaching 28.52 g/L. Finally, the precursor neohesperidin was integrated with a chemical conversion system leading to the establishment of an efficient biochemical process for high-yield NHDC production at an industrial scale. Our findings provide a roadmap for sustainable production of high-value flavonoids and their derivatives.

INTRODUCTION

The increasing global prevalence of obesity and diabetes has accelerated the development of non-nutritive sweeteners.[1-4] Neohesperidin dihydrochalcone (NHDC), a natural low-calorie sweetener,[5] exhibits a sweetness potency 1,000–1,500 times greater than that of sucrose.[6] Distinct from conventional artificial sweeteners, NHDC not only avoids inducing systemic inflammation and fatty liver development in murine models,[4] but also exhibits significant therapeutic potential due to its antioxidant, hepatoprotective, anti-inflammatory, and anti-apoptotic properties.[7] Furthermore, owing to its remarkable bitter-masking capacity and synergistic effects with other sweeteners,[8-10] it has been approved as a food and drug additive in many countries and regions. However, the industrial-scale production of NHDC continues to face significant constraints, primarily due to inherent limitations in the conventional alkaline-mediated ring-opening synthesis process using neohesperidin, a flavonoid extracted from citrus fruits, as the precursor substrate, whose exceptionally low natural abundance in citrus sources creates severe supply chain bottlenecks and ultimately restricts scalable production capabilities.[11,12] Although the industrial production process for NHDC has been in place since the 1980s, the severe scarcity of raw materials has rendered plant extraction incapable of meeting market demand.

The biosynthesis of neohesperidin requires an extensive 13-step enzymatic cascade within the phenylpropanoid pathway (Figure 1). The initial biosynthetic pathway from L-tyrosine or L-phenylalanine to naringenin has been well established in previous studies.[13] Subsequently, naringenin is converted to hesperetin through sequential catalysis by flavonoid 3`-hydroxylase (*F3`H*) and flavonoid 4`-*O*-methyltransferase (*F4`OMT*).[14] Hesperetin is further modified through two glycosylation steps mediated by flavonoid 7-*O*-*β*-glucosyltransferase (*F7GlcT*) and 1, 2-rhamnosyltransferase (*1,2RHAT*), yielding the final product neohesperidin.[15] Although heterologous biosynthesis of naringenin has achieved remarkable titers of 8.65 g/L in engineered systems,[16] the production efficiency of hesperetin remains significantly lower (178.2 mg/L).[17] This bottleneck primarily arises from the catalytic promiscuity and suboptimal activity of F4`OMT, which severely limits the heterologous biosynthesis of neohesperidin.[18]

Yarrowia lipolytica can utilize diverse carbon sources, particularly glycerol, fatty acids, and alkanes, which are suitable for industrial production.[19] Various flavonoids have been successfully synthesized in engineered *Y. lipolytica* strains, and previous studies have shown that *Y. lipolytica* can provide sufficient UDP-glucose (UDPG) as a precursor.[16,20,21] In this study, we engineered *Y. lipolytica* to achieve enhanced *de novo* biosynthesis of neohesperidin, which was subsequently integrated with a chemical conversion system to establish a scalable biochemical process for high-yield NHDC production at an industrial scale.

MATERIALS AND METHODS

Genetic manipulation for the construction of plasmids and strains

Candidate genes for the biosynthesis pathway of neohesperidin and *MCR-C*, *BeuA*, *BbPK* and *EcPTA* were synthesized by GenScript (Nanjing, China) with codon optimization for different strain. Endogenous genes *YlOMT*, *SAHH*, *ADO*, *ALAS*, *YlCYB5*, *ARO1*, *ARO2*, *ARO3*, *ARO4* and *ARO7* were amplified from *Y. lipolytica* genomic DNA. All strains used here are listed in Table S1. All the vectors described in this paper were constructed through Gibson assembly are listed in Table S2. All the fragments used for overexpression of genes were amplified by PCR using primers as described in Table S3. Amino acid sequences of functional genes used to construct engineering strains are listed in Table S4. Cloning was performed with chemically competent *Escherichia coli* strain DMT.

Saccharomyces cerevisiae strain W303-1B was used for characterization of candidate genes involved in neohesperidin biosynthesis pathway from naringenin. Head-to-head promoters (pPGK1-pTDH3), *ATR2* and candidate *F3`Hs* were cloned into Y22-TC. To optimize the expression of P450s, we truncated the transmembrane domains of *CsF3`H* and *ATR2* and constructed a fusion protein. However, none of these strategies led to an improvement in eriodictyol production (Figure S1). Candidate *OMTs* and *UGTs* were cloned into Y33-PE separately. The modularized two-step (M2S) integration method was used for chromosome integration. T-Series vectors were used to construct integrative plasmids. The expression vector with homologous arms was amplified and transformed with selection marker Lue2 into PC1 at integration site *YORWΔ15* to realize gene integration generating strain SC48. Due to the fact that the main way of repairing double strand breaks in *Y. lipolytica* is through non-homologous end joining (NHEJ). To increase the efficiency of homologous recombination, *Y. lipolytica* strain W29 that was knocked out *KU70* related to NHEJ repair mechanism and *Cas9* gene was integrated. *Y. lipolytica* strain W29 *ΔKU70* (*MATa KU70Δ::PrTEF1-cas9-TTef12::PrGPD-hyg-TLip2*) was used as the parent strain for all engineered strain here. A single gRNA plasmid and integrative plasmid were applied as the basis for constructing integrative strains through CRISPR/Cas9 system. The detailed construction process and integration methods could be found in the previous work.[22]

The full-length of *CsOMT-15* and *YlOMT* with C-terminal hexahistidine (6×His) tag were cloned into pCWOri (+) and pET28a (+) vector forming plasmids, pCWOri (+)-*CsOMT-15* and pET28a (+)-*YlOMT* respectively. These

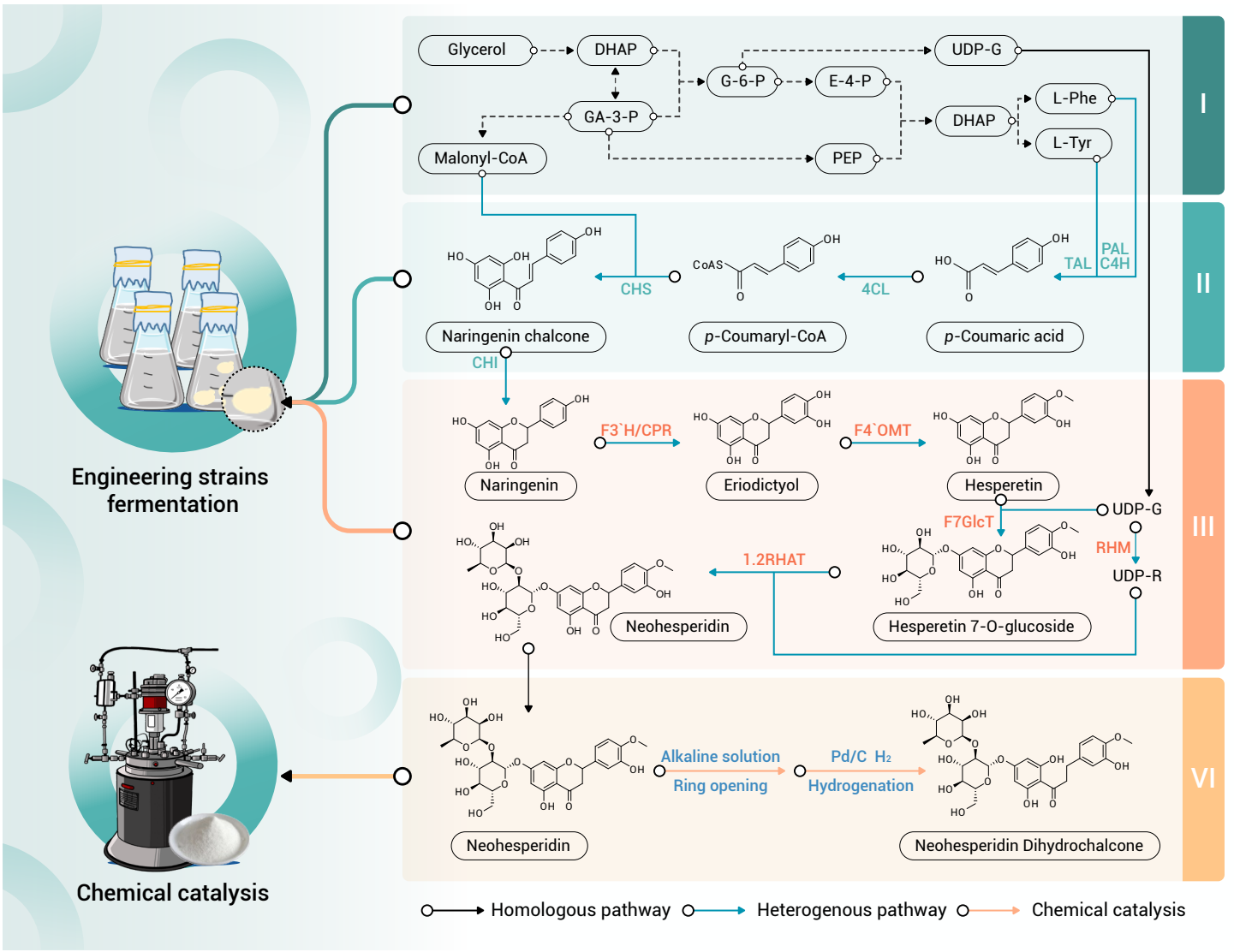

Figure 1. Biochemical coupling synthesis of NHDC Module I (precursor supply module, dark green label) is to provide the precursor malonyl-CoA, *p*-coumaric acid and UDP glucose from glycerol. Reconstruction of the neohesperidin synthesis pathway by introducing Module II (naringenin synthesis module, light green label) and Module III (neohesperidin synthesis module, orange label). Module IV (chemical reaction module, yellow label) is chemical conversion of neohesperidin to synthesize NHDC. DHAP dihydroxyacetone phosphate, GA-3-P Glyceraldehyde-3-phospate, G6P Glucose-6-phospate, E4P erythrose 4-phosphate, PEP phosphoenolpyruvate, DAHP 3-deoxy-D-arabino-heptulosonic acid 7-phosphate, L-Tyr L-tyrosine, L-Phe L-phenylalanine, UDP-G UDP-glucose, UDP-R UDP-rhamnose. *TAL* tyrosine ammonia-lyase, *PAL* phenylalanine ammonia-lyase, *C4H* cinnamate-4-hydroxylase, *4CL* 4-coumaroyl-CoA-ligase, *CHS* chalcone synthase, *CHI* chalcone isomerase, *F3`H* flavonoid 3`-hydroxylase, *CPR* cytochrome P450 reductase, *F4`OMT* flavonoid 4`-*O*-methyltransferase, *F7GlcT* flavonoid 7-*O*-*β*-glucosyltransferase *1, 2RHAT* 1, 2-rhamnosyltransferase, *RHM* rhamnose synthase.

expression vectors were then transformed into *E. coli* BL21 (DE-3).

Media and growth conditions

Yeast nitrogen base without amino acids and ammonium sulfate (YNB), amino acids, adenine, peptone, tryptone, yeast extract, $(NH_4)_2SO_4$, $MgSO_4{\cdot}7H_2O$, KH_2PO_4, K_2HPO_4, NaCl, $MgCl_2$, trace metals and vitamins in MM medium, glucose, glycerol, imidazole, isopropyl-*β*-D-thiogalactopyranoside (IPTG), PEG3350, PEG4000, LiAc and ssDNA were purchased from Solarbio. Kanamycin and ampicillin were purchased from Sigma-Aldrich, USA. Authentic reference standards of flavonoids were purchased from Yuanye Bio-Technology. Nourseothricin was purchased from Mei5 Biotechnology

E. coli were cultured in LB at 37 °C with appropriate antibiotic. *S. cerevisiae* strains were grown in the corresponding nutritionally deficient media at 30 °C. Transformation of *Y. lipolytica* cells were grown on the YPD plates with 250 mg/L nourseothricin. YP and MM medium was used for shake-flask fermentation of *Y. lipolytica*[23] and the concentration of carbon source varies from 10 g/L-40 g/L (Figure S2). All yeast strains were grown in 24-well plate containing 3 mL medium and at 30 °C, 500 rpm to an OD_{600} of approximately 1.0. The seeds were inoculated into 250 mL flasks containing 50 mL medium were to an OD_{600} of 0.05 and were grown at 30 °C, 220 rpm for 3-4 days.

Heterologous expression and enzyme assay of *CsOMT-15* and *YlOMT*

Engineered strains were grown in LB medium at 37°C supplemented with 100 mg/L of respective antibiotic (kanamycin for pET28a (+) and ampicillin for pCWOri (+) vector) until the OD_{600} reached between 0.6-0.8. Recombinant protein was then induced with 1mM IPTG at 16°C for 20 h. Induced bacterial cells were harvested by centrifugation at 5000×g for 10 min. Then, the cells were lysed in lysis buffer (0.1 M PBS, 10% glycerol (v/v)) using a high-pressure homogenizer (JNBIO, China) and the supernatant (10,000×g, 60 min) was then subjected to Ni^{2+}-chelating affinity chromatography column that was preconditioned with the same lysis buffer. After washing the column with 40 mL wash buffer (0.1 M PBS, 10% glycerol, 50 mM imidazole), 40 mL elution buffer (0.1M PBS, 10% glycerol, 250 mM imidazole) was used to elute the OMTs. The eluted OMTs was dialyzed against lysis buffer (0.1 M PBS, 10% glycerol (v/v)) using ultrafiltration centrifugal columns (Millipore, USA). Purified proteins were verified with 12% SDS-PAGE and the concentration was estimated with BCA Protein Assay Reagent Kit (Pierce, USA).

Recombinant enzymes *CsOMT-15* and *YlOMT* were incubated with eriodictyol to explore their activities. In a final volume of 200 μL, 40 μg of purified enzyme, 10 mM $MgCl_2$, 200 μM SAM and 200 μM eriodictyol were added in 0.1 M NaAc buffer (pH = 4.5-6.0), 0.1 M PBS buffer (pH = 6.0-7.5) and 0.1 M

Tris-HCl buffer (pH = 7.5-9.0) containing 10% glycerol (v/v). Assays were carried out for 1 h at 30°C and stopped with equal volume methanol with 10% H_2SO_4 (v/v).

Protein modeling, docking, and electrostatic analysis

The three-dimensional structure of *YlOMT* and *CsOMT-15* were predicted using AlphaFold2 with the default settings. To guide substrate and cofactor placement, we referred to the crystal structure of a related O-methyltransferase (PDB ID: 1SUI), in which the positions of the methyl donor SAH and a phenolic substrate are resolved. Based on this reference, we employed GNINA (v1.0) to dock SAM as the methyl donor and eriodictyol as the acceptor ligand into the AlphaFold2-predicted OMT models. A Ca^{2+} ion was manually placed at the conserved metal coordination site, guided by the spatial arrangement in 1SUI, and its position was refined during energy minimization. The resulting ternary complexes were subjected to energy minimization using the OpenMM toolkit under the AMBER force field (ff14SB for proteins, GAFF for small molecules, and standard ion parameters for Ca^{2+}). Ligand parameters were generated using the Antechamber module in AmberTools. To assess the protonation states and potential catalytic relevance of charged residues under acidic conditions, we estimated the pKa values of ionizable amino acids in the minimized complexes using PropKa v3.5.

Fed-batch fermentation in 5-L, 200-L, and 5000-L bioreactor

For 5-L fermentation production of naringenin and neohesperidin, seed culture medium was cultured in 250 mL flasks containing 50 mL MM medium at 30°C, 220 rpm for 24 h. Then seed culture medium was inoculated into a 5-L bioreactor (Shanghai Baoxing Bio-engineering Equipment Co., Ltd) with 2 L MM medium containing 20 g/L glycerol, 5 g/L KH_2PO_4, 5 g/L $(NH_4)_2SO_4$, 0.8 g/L $MgSO_4{\cdot}7H_2O$, 2.5 mL/L trace metal solution and 1.5 mL/L vitamin solution. Dissolved oxygen was controlled at 20% (production of naringenin) or 40% (production of neohesperidin) by agitation speed (200-900 rpm) and ventilation flow rate (1.5 L/min), pH was controlled at 5.0 (production of naringenin) or 5.5 (production of neohesperidin) by adding 28% $NH_3{\cdot}H_2O$, and the fermentation temperature was controlled at 30 °C throughout the entire fermentation process. After 12 h, the feeding medium consisting of 800 g/L glycerol was continuously added into bioreactor (feeding speed was sustained at 6-10 mL/h).

For 200-L fermentation production of neohesperidin, seed culture medium was cultured in 3 L shake-flask comprising 1 L MM medium at 30°C, 220 rpm for 24 h. Then seed culture medium was inoculated into a 200-L bioreactor, and initial fermentation medium was consistent with the 5-L bioreactor. Agitation speed (100-400 rpm) ventilation flow rate (30-50 L/min) controlled dissolved oxygen at 40%. The feeding speed was 40 times faster than that of 5-L bioreactor. Other parameters were consistent with the 5-L bioreactor.

For 5000-L fermentation production of neohesperidin, cultivation method of the first-class seed was consistent with the 200-L seed cultivation method. Then the first-class seed culture medium was inoculated to a 500-L fermenter for 24 h. Subsequently, the secondary seed was transferred to a 5000-L fermentation tank. Dissolved oxygen was controlled at 40% by ventilation flow rate (0.5 vvm) and agitation speed (150 rpm). Start feeding after dissolved oxygen and pH rose, and feeding speed was cntroled at 6600 g/h (800 g/L glycerol). Initial fermentation medium without nitrogen source and other parameters were consistent with the 5-L bioreactor.

Product extraction and quantification

For the extraction of flavonoid compounds, an equal volume of methanol was mixed with fermentation broth and the mixture was sonicated for 30 min. After centrifugation at 12,000 ×g for 15 min, the supernatant was used for analyzed. HPLC and LC-MS assays were the same as described before.[24]

For the separation and purification of neohesperidin from fermentation broth. First, adjust the pH of the fermentation broth to 11.0 using sodium hydroxide, and stir at 60°C for 2 h. The extract was filtered while hot, and the filtrate was cooled to room temperature. Then, citric acid was slowly added dropwise to pH 4.0 to precipitate crude neohesperidin. Static at 4 °C for 12 h, filter and collect the precipitate, wash with distilled water until neutral. The crude product was mixed with 70% ethanol at a ratio of 1:50 (w/v), followed by the addition of 3% (w/v) activated carbon for decolorization. After filtration, the solution was allowed to stand for 12 h to facilitate crystallization. The resulting white needle-shaped crystals were collected by filtration. Crystallization is vacuum dried to constant weight in a vacuum dryer to obtain pure neohesperidin.

Chemical reaction catalyzes the formation of NHDC from neohesperidin

Considering the cost and operational difficulty, alkaline extraction and acid precipitation was used to separate and purify neohesperidin from fermentation broth. 5 g purified neohesperidin was weighed and dissolved in 4.8% (w/v) sodium hydroxide solution and the resulting mixed solution was magnetically stirred at 70°C for 2 h. After cooling, 1.1 g palladium-on-charcoal (Pd /C) was added into the mixed solution and the air in the reaction system was replaced with hydrogen for three times. The reaction was carried out at 30°C for 48 h under atmospheric pressure. After the end of the reaction was aspirated and filtered, the filtrate was taken to adjust the pH to neutral using concentrated hydrochloric acid. The crystals were then crystallized at 4°C for 72 h, and the white cake obtained after filtration was that of NHDC crude.

RESULTS

Elucidation of neohesperidin biosynthesis pathway

We first screened candidate genes in the biosynthetic pathway from naringenin to neohesperidin in *S. cerevisiae*. The eriodictyol synthesis pathways from naringenin were constructed by combining five cytochrome P450s with *ATR2*, cytochrome P450 reductase (*CPR*) from *Arabidopsis thaliana* (Figure S3).[25-28] *CsF3`H* from *Citrus sinensis* exhibited the best hydroxylation activity (Figures 2A & S3). Then, we proposed to resolve the rate-limiting step in the pathway by obtaining 24 candidate *OMTs* in *C. sinensis* based on genomic, transcriptomic and modeling analysis (Table S5), as well as four known plant-derived *OMTs*.[29-32] However, only *CsOMT-15*, *CsOMT-18*, *CsOMT-21* from *C. sinensis* and *CCoAOMT* from *A. thaliana* catalyzed the 4`-*O*-methylation of eriodictyol to produce hesperetin, where *CsOMT-15* exhibited the highest activity (Figures 2A & S4). According to previous reports,[33-35] six *F7GlcTs* were selected to evaluate their activity toward hesperetin using a UDPG-producing strain PC1,[36] indicating that *CsUGT* from *C. sinensis* exhibited the highest efficiency in converting hesperetin to hesperetin 7-*O*-glucoside (Figures 2A & S5). Finally, *CsF3`H*, *ATR2*, *CsOMT-15*, *CsUGT*, rhamnose synthase from *A. thaliana* (*AtRHM1*), and *Cm1,2RHAT* from *Citrus maxima* were introduced into *S. cerevisiae*, which produced 35.19 mg/L (0.06 mM) neohesperidin when fed with 0.6 mM naringenin (Figure 2E).

In order to further improve the productivity of neohesperidin, we proposed to transfer the biosynthetic pathway into *Y. lipolytica*. Surprisingly, when we integrated the combination of *CsF3`H* and *ATR2* (YL1, *Y. Lipolytica* strain 1), we detected not only eriodictyol but also hesperetin by feeding naringenin, indicating that an endogenous *OMT* may catalyze the methylation of eriodictyol at the 4` position (Figure S6). Indeed, knocking out the coding gene in *Y. lipolytica* (here named *YlOMT*, strain YL2) abolished hesperetin production by feeding eriodictyol (Figures 2B & S6). The function of *YlOMT* on eriodictyol was also proved by enzyme assays *in vitro* (Figure 2C). To compare the activities of *YlOMT* and *CsOMT-15*, we overexpressed them in *Y. lipolytica* and the titer of hesperetin in the strain with *YlOMT* (YL3) was improved by 14.85% comparing to the strain containing *CsOMT-15* (YL4) (Figure 2B). In addition, *CsOMT-15* was inactive at pH < 5.0, whereas *YlOMT* exhibited higher activity under acidic conditions *in vitro* (Figure 2C). This pH tolerance may partially explain the superior intracellular efficiency of *YlOMT* in *Y. lipolytica* because the low intracellular pH environment in yeast (pH < 6.0) attributed to acidic metabolite production.[37] To further investigate the molecular basis of this pH-dependent activity, we analyzed the key residues in the active site of the *OMTs*. Structural modeling revealed that *YlOMT* contains two aspartic acids residues that coordinate with Ca^{2+}, which is crucial for the catalytic process by providing the environment for substrate deprotonation. These two residues (166D and 194D) exhibit low predicted pKa values (2.08 and 0.89, respectively, estimated by PropKa), allowing them to remain negatively charged state even under acidic conditions (Figures 2D & S7). Therefore, we integrated the biosynthesis pathway of neohesperidin using endogenous *YlOMT*, producing 123.46 mg/L (0.2 mM) neohesperidin with feeding 0.6 mM naringenin (YL6). The yield was about 3.51-fold that of *S. cerevisiae*

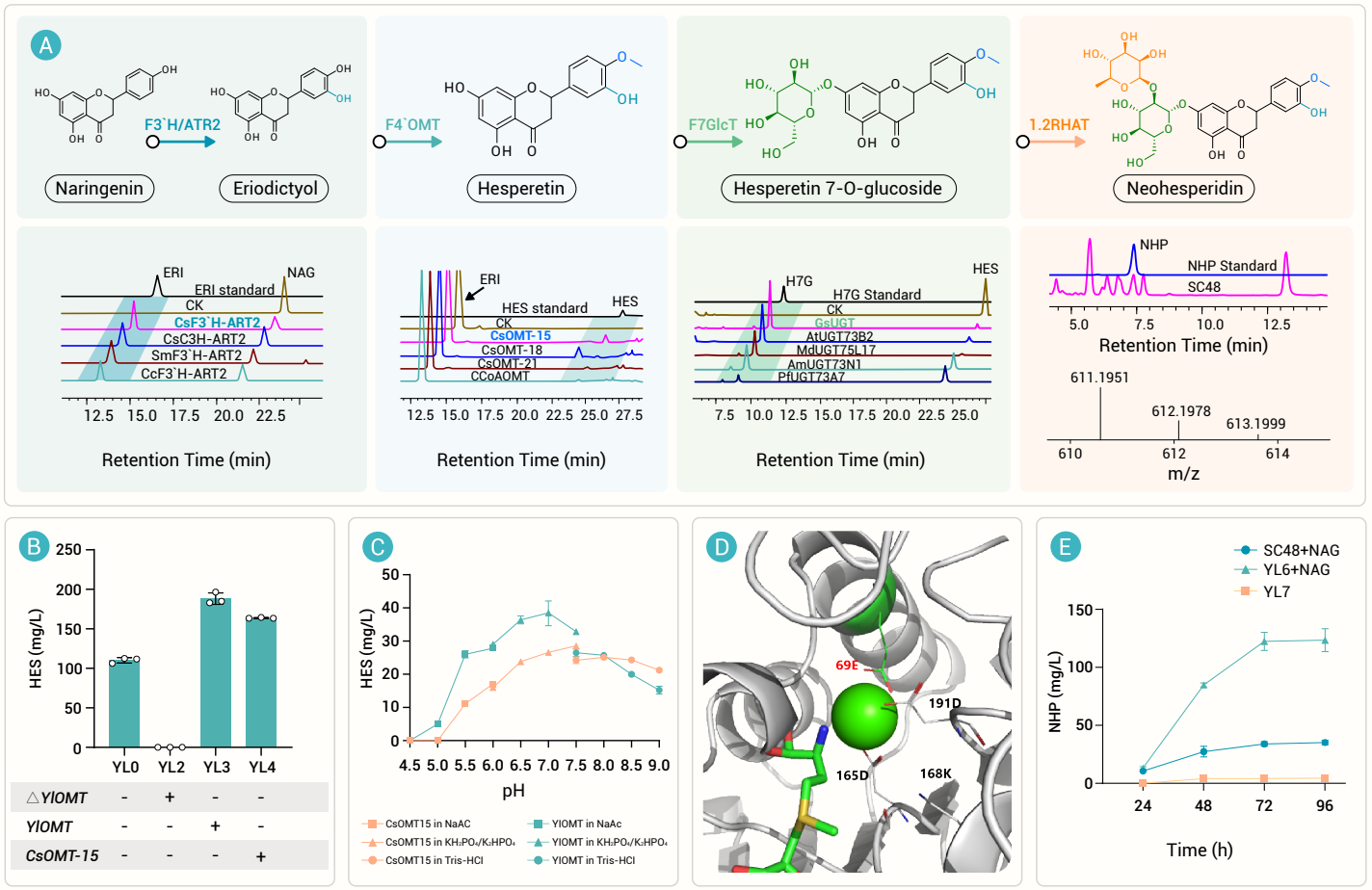

Figure 2. Elucidation and heterologous reconstruction of the neohesperidin synthesis pathway in yeast (A) HPLC results of the characterization of *F3`Hs* towards naringenin, *F4`OMTs* towards eriodictyol, *F7GlcTs* towards hesperetin and LC-MS analysis of neohesperidin biosynthesis in *S. cerevisiae* feeding naringenin. CK represents negative control strain. (W303-Y22 was used for *F3`H* characterization, W303-Y33 was used for *F4`OMT* characterization and PC1-Y33 was used for *F7GlcT* characterization. Y22 and Y33 is the abbreviation of plasmid YCPlac22 and YCPlac33, respectively.) NAG naringenin; ERI eriodictyol; HES hesperetin; H7G hesperetin 7-*O*-glucoside; NHP neohesperidin. *CsF3`H* from *Citrus sinensis*, *CclF3`H* from *Citrus clementina*, *SmF3`H*$^{D285N}$ from *Silybum marianum*, *CcF3`H* from *Callistephus chinensis*, *CsC3H* (chalcone 3-hydroxylase) from *Cosmos sulphureus* and *ATR2* from *Arabidopsis thaliana*. *CCoAOMT-7* from *A. thaliana*. *PfUGT73A7*, *PfUGT88A7* from *Perilla Frutescens*, *AmUGT73N1* from *Antirrhinum majus*, *AtUGT73B2* from *A. thaliana*, *MdUGT75L17* from *Malus domestica* and *CsUGT* from *C. sinensis*. For other abbreviations, please refer to Figure 1 legend. (B) Discovery of endogenous F4`OMT (*YlOMT*) of *Y. lipolytica* and comparison of activity with *CsOMT-15 in vivo*. (C) Enzymatic activities of *YlOMT* and *CsOMT-15* towards eriodictyol at different pH. The reaction pH was controlled by different buffer, i. e. 0.1 M NaAc buffer (pH 4.5–6.0), 0.1 M KH_2PO_4/K_2HPO_4 buffer (pH 6.0–7.5) and 0.1 M Tris-HCl buffer (pH 7.5–9.0). (D) Comparison of key residues of *YlOMT* and *CsOMT-15* in reaction centers. (E) The *de novo* production of neohesperidin in YL7 and comparison neohesperidin yield in *S. cerevisiae* and *Y. lipolytica* feeding naringenin. *S. cerevisiae* strains were cultivated in corresponding defective medium and *Y. lipolytica* strains were cultivated in MM medium with 20 g/L glucose. All data are presented as mean of n = 3 biologically independent samples and error bars show the standard deviations. The circles represent individual data. Source data are provided as a Supplementary Table.

(Figure 2E). However, multiple glycosylation by-products of intermediate were detected indicating the hybridization of glycosyltransferases and excess supply of UDPG in *Y. lipolytica* (Figures S2 & S8). In order to realize *de novo* biosynthesis of neohesperidin in *Y. lipolytica*, a naringenin biosynthesis pathway comprising *FjTAL*, tyrosine ammonia-lyase (*TAL*) from *Flavobacterium johnsoniae*, along with *Eb4CL*, 4-coumaroyl-CoA-ligase (*4CL*) and *EbCHS*, chalcone synthase (*CHS*) from *Erigeron breviscapus*, was integrated into YL6 to generate YL7. However, the achieved yield (only 4.4 mg/L) was significantly lower than the above yield by feeding naringenin, indicating insufficient supply of the naringenin precursor (Figure 2E).

Construction of a high-yield naringenin-producing strain

The low activity of heterologous enzymes is one of the major obstacles in the heterologous biosynthesis of flavonoids.[38] To construct a high-yield naringenin-producing strain for neohesperidin biosynthesis, we screened three key enzymes, phenylalanine ammonia-lyase (*PAL*), *TAL* and *CHS* involved in naringenin biosynthesis pathway (Figure 3A), which were often regarded as the rate-limiting enzymes in flavonoid production.[39] *RgPAL* from *Rhodotorula glutinis*[40] and *EbPAL* from *E. breviscapus*, which was previously demonstrated to be effective for scutellarin production in our earlier work,[22] were used to assess the productivity of cinnamic from phenylalanine. At the same time, we observed *p*-coumaric acid accumulation (Figure S9). Therefore, to accurately evaluate the activity of two *PALs*, *ATR2*, *YlCYB5* (*Y. lipolytica* endogenous *cytochrome b5*) and *EbC4H*, cinnamate-4-hydroxylase (*C4H*) from *E. breviscapus* were introduced and the yield of *p*-coumaric acid in the strain with *RgPAL* (182.96 mg/L) was 4.24 times higher that of the strain with *EbPAL* (43.12 mg/L) (Figure 3B). Next, six *TALs* were individually integrated into *Y. lipolytica* to produce *p*-coumaric acid from tyrosine based on enzyme kinetic parameters (Table S6). Although *RcTAL* from *Rhodobacter capsulatus* DSMZ 1710 possessed the highest catalytic activity *in vitro*, *CluTAL* from *Chryseobacterium luteum sp. nov* exhibited the best performance in *Y. lipolytica* with a yield of 168.26 mg/L *p*-coumaric acid (Figure 3C). Finally, seven *CHSs* from the previous studies were used to screen.[24,41-46] *MdCHS2* from *Medicago sativa* (184.07 mg/L) demonstrated the highest activity (Figure 3D). Previous studies showed that the *CHS*^{T132G} mutant exhibited enhanced catalytic activity compared to the wild-type enzyme.[47] Unfortunately, we did not detect higher activity for the mutant *MdCHS2*^{T132G} (Figure 3D). Based on these enzymes that show higher efficiency in *Y. lipolytica*, we constructed a robust platform strain enabling naringenin production from both L-tyrosine and L-phenylalanine, reaching a titer of 188.51 mg/L (Figure S10). However, the synergistic enhancement between the two pathways remains modest, as the flavonoid synthetic pathway is constrained by downstream enzymes and additionally regulated by the upstream shikimate pathway.

Figure 3. Engineered metabolic pathway for the *de novo* biosynthesis of naringenin in *Y. lipolytica* (A) Overview of *Y. lipolytica* metabolic pathway for naringenin biosynthesis. PPA prephenate, *P*-CA *p*-coumaric acid, CA cinnamic acid, *P*-CA-CoA *p*-coumaroyl-CoA. *CluTAL* from *Chryseobacterium luteum sp. nov*, *RgPAL* from *Rhodotorula glutinis*, *EbC4H* from *E. breviscapus*, *YlCYB5* (*cytochrome b5*) from *Y. lipolytica*, *Eb4CL* from *E. breviscapus*, *MdCHS2* from *Medicago sativa*, *EbCHI* from *E. breviscapus* were used for naringenin production, which are represented in orange. Overexpressed *Y. lipolytica* endogenous pathway genes are shown in black, including acetyl-CoA carboxylase (*ACC1*), L-tyrosine-feedback-insensitive DAHP synthase mutant ($ARO4^{K221L}$), L-tyrosine-feedback-insensitive chorismate mutase ($ARO7^{G139S}$), pentafunctional aromatic protein (*ARO1*), chorismate synthase (*ARO2*) and DAHP synthase (*ARO3*). For other abbreviations, please refer to Figure 1 and Figure 2 legend. (B) Modification of the intermediate *p*-coumaric acid engineering strain. *EbPAL* from *E. breviscapus*. (C) Screening of highly active *TAL* in *Y. lipolytica*. *StsTAL* from *Streptomyces sp. NRRL F*-4489, *RpcTAL* from *Rivularia sp. PCC* 7116, *RcTAL* from *Rhodobacter capsulatus DSMZ* 1710, *RgTAL* from *Rhodotorula glutinis*, *FjTAL* from *Flavobacterium johnsoniae*. (D) Screening of highly active *CHS* in *Y. lipolytica*. *EbCHS* from *E. breviscapus*, *AtCHS* from *A. thaliana*, *PcCHS* from *Polygonum cuspidatum*, *HaCHS* from *Hypericum androsaemum*, *InCHS-D* from *Ipomoea nil*, *RaCHS* from *Rheum australe*. (E) Modification of the shikimic acid pathway in engineering strain. (F) Modification of limited enzyme copy number and supply of malonyl CoA in engineering strain. Phosphoketolase from *Bifidobacterium brebifidum* (*BbPK*), phosphotransferase from *E. coli* (*EcPTA*) and *Y. lipolytica* endogenous Acetyl-CoA carboxylase (*ACC1*) were overexpressed for increasing supply of malonyl-CoA. All strains were cultivated in 250 mL shake flasks containing 50 mL of YPD medium. All data are presented as mean of n = 3 biologically independent samples and error bars show the standard deviations. The circles represent individual data. Student's t-test was used for comparing two groups (*p < 0.05, **p < 0.01, ***p < 0.001). Source data are provided as a Supplementary Table.

To enhance metabolic flux toward naringenin synthesis, the feedback inhibition-resistant mutant alleles $ARO4^{K221L}$ and $ARO7^{G139S}$ were introduced (YL30) to relieve L-tyrosine-mediated feedback inhibition. Although the naringenin titer in the resulting strain (YL31) did not increase, the titer of *p*-coumaric acid reached 1213.96 mg/L (Figure 3E). Moreover, the shikimate pathway flux in *Y. lipolytica* is primarily regulated by *ARO4* and *ARO7* since overexpression of *ARO1*, *ARO2*, and *ARO3* did not enhance *p*-coumaric acid or naringenin production (Figure 3E). In order to further enhance the conversion from *p*-coumaric acid to naringenin, we attempted to simultaneously increase the copy number of *Eb4CL* and *MdCHS2*. The naringenin titer reached 473.91 mg/L when the copy number of *Eb4CL* and *MdCHS2* were increased simultaneously to four (Figure 3F). In addition, we observed the

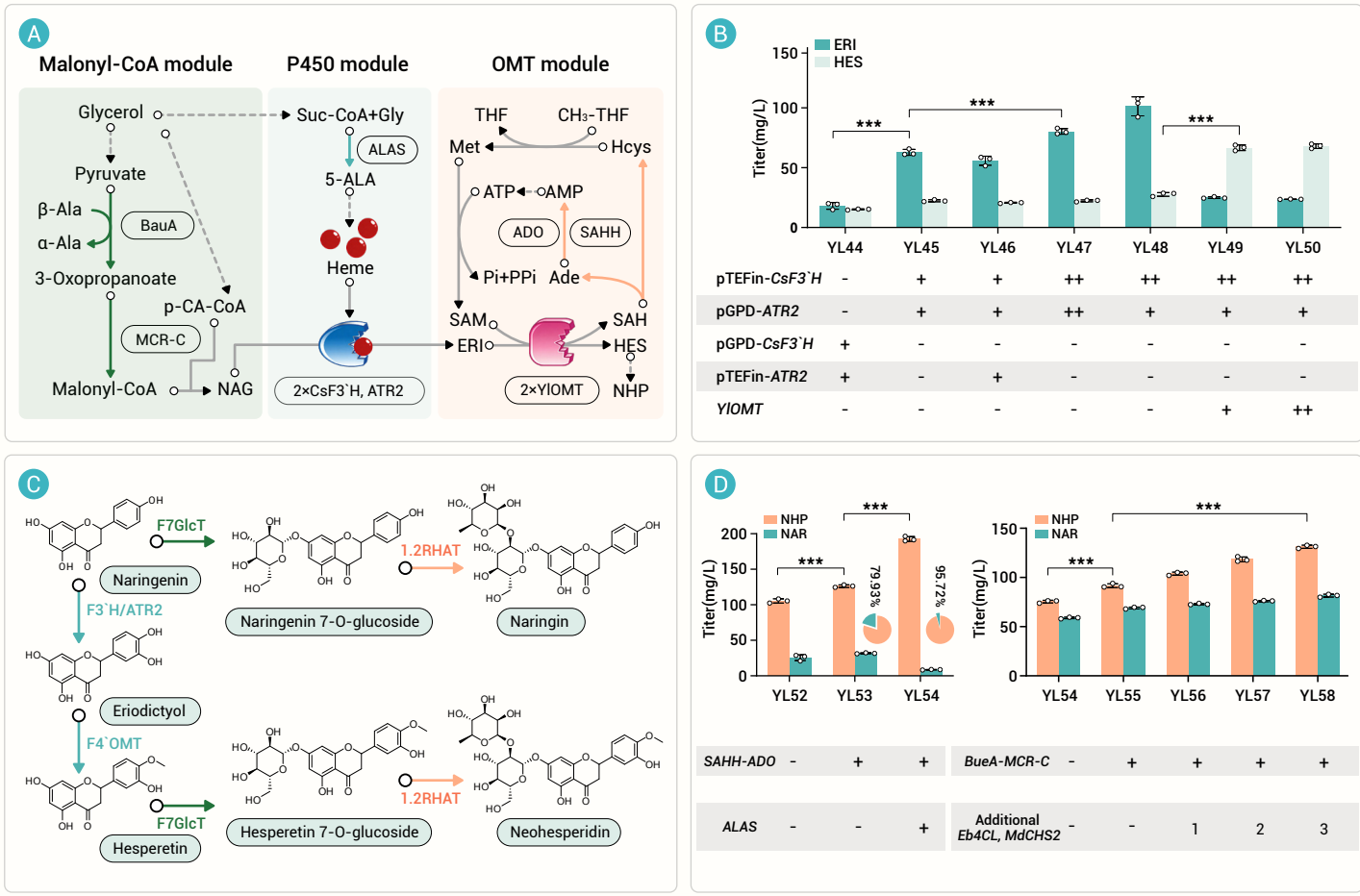

Figure 4. Engineering for efficient production of neohesperidin in *Y. lipolytica* (A) Scheme of the engineered metabolic pathway for neohesperidin biosynthesis. Dark green arrow: NCM pathway was induced into engineered strain to increase malonyl-CoA supply and reduce carbon losses. Light green arrow: Optimization of P450 enzyme and CPR copy number and enhancement of heme supply were applied to promote the conversion of NAG to ERI. Orange arrow: Eliminating the rate-limiting step in the *OMT*-catalyzed synthesis of HES through SAM regeneration and increasing the copies of *YlOMT*. NCM non-carboxylative malonyl-CoA, *β*-Ala *β*-alanine, *α*-Ala *α*-alanine, Suc-CoA, succinyl-CoA, Gly glycine, 5-ALA 5-aminolevulinic acid, SAM S-adenosylmethionine, Met methionine, Hcys homocysteine, SAH S-adenosylhomocysteine, THF tetrahydrogen folic acid, CH_3-THF 5-methyl tetrahydrogen folic acid, ATP adenosine triphosphate, AMP adenosine monophosphate, Ade adenosine. *BauA* *β*-alanine-pyruvate transaminase from *Pseudomonas aeruginosa*, *MCR-C* C-terminal fragment of malonyl-CoA reductase from *Chloroflexus aurantiacus*, *ALAS* 5-ALA synthase, *ADO* adenosine kinase, *SAHH* SAH hydrolase, *YlOMT* F4`OMT identified in *Y. lipolytica*. For other abbreviations, please refer to Figure 1 and Figure 2 legend. (B) Replacing the promoter pGPD of *CsF3`H* with pTEFIN and overexpression of *CsF3`H* and *YlOMT* increased ERI and HES production. (C) The biosynthesis pathway of naringin and neohesperetin. (D) Increase the supply of cofactors and precursor supply for neohesperidin production. NAR Naringin. All strains were cultivated in 250 mL shake flasks containing 50 mL of MM medium with 10 g/L glycerol except for the strains YL54-58, which were cultivated with 20 g/L glycerol. All data are presented as mean of n = 3 biologically independent samples and error bars show the standard deviations. The circles represent individual data. Student's t-test was used for comparing two groups (*$p < 0.05$, **$p < 0.01$, ***$p < 0.001$). Source data are provided as a Supplementary Table.

degradation of *p*-coumaric acid and cinnamic acid in *Y. lipolytica* cultured in minimal medium, which might be mediated by the CoA-dependent *β*-oxidation pathway (Figures S11-S12).[48] Thus, the multifunctional *β*-oxidation hydratase/dehydrogenase (*MFE1*) was knocked out in wild type strain and engineered strain YL40. Although the knockout strain eliminated the consumption of *p*-coumaric acid and cinnamic acid, the production of naringenin decreased instead (Figures S11 & S13). This phenomenon may be attributable to the diversion of carbon fluxes due to competitive metabolic demands. Finally, we conducted fermentation tests using strain YL40 in a 5-L fermenter with glycerol as the carbon source. The yield of naringenin reached 8.87 g/L after 156 h, however, the strain YL40 exhibited a significantly lower OD_{600} (Figure S14). This phenomenon could be attributed to the cytotoxicity of flavonoids, which can be reduced by glycosylating the product.[49]

Metabolic engineering of neohesperidin producing strain

With the advancement of naringenin biosynthesis, we were committed to refining the biosynthetic pathway of neohesperidin (Figure 4A). Initially, *CsF3`H* and *ATR2* were integrated into YL40, but the low yield of eriodictyol (18.07 mg/L) revealed that hydroxylation is a rate-limiting step (Figure 4B). To eliminate this bottleneck, the expression intensity and ratio of P450 to CPR were optimized. The catalytic activity of the two genes on naringenin under different promoters was compared. The yield of eriodictyol in the fermentation product of YL45 (pTEFin-*CsF3`H* and pGPD-*ATR2*) reached 62.75 mg/L, which was 3.47-fold that of YL44 (pTEFin-*ATR2* and pGPD-*CsF3`H*). This indicated that the expression of *CsF3`H* under a strong promoter was more conducive to the production of eriodictyol (Figure 4B). We further increased the copy number of P450 and CPR to enhance eriodictyol production. It has been reported that increasing the ratio of P450 to CPR in heterologous hosts is beneficial for better simulating its state in natural hosts.[50] Thus, YL46 (with additional *ATR2*), YL47 (with additional *CsF3`H* and *ATR2*) and YL48 (with additional *CsF3`H*) were constructed. Comparing with the starting strain YL45, the eriodictyol titer increased 61.37% in YL48 (101.26 mg/L) and 27.94% in YL47 (80.28 mg/L) (Figure 4B). The lower yield of YL46 might be due to the cytotoxicity caused by overexpression of CPR. Then, the strain YL48 was engineered to generate strain YL49 by overexpressing *YlOMT*. The yield of hesperetin increased from 27.67 mg/L to 66.67 mg/L (Figure 4B). We attempted to introduce additional copies of *YlOMT* into strain YL49 to reduce the accumulation of eriodictyol. However, the production of hesperetin was not significantly improved (67.99 mg/L) (Figure 4B). Finally, two glycosylation steps were integrated to create strain YL52, resulting in a neohesperidin titer of 105.38 mg/L (Figure 4D).

To further enhance the neohesperidin yield and reduce by-product accu-

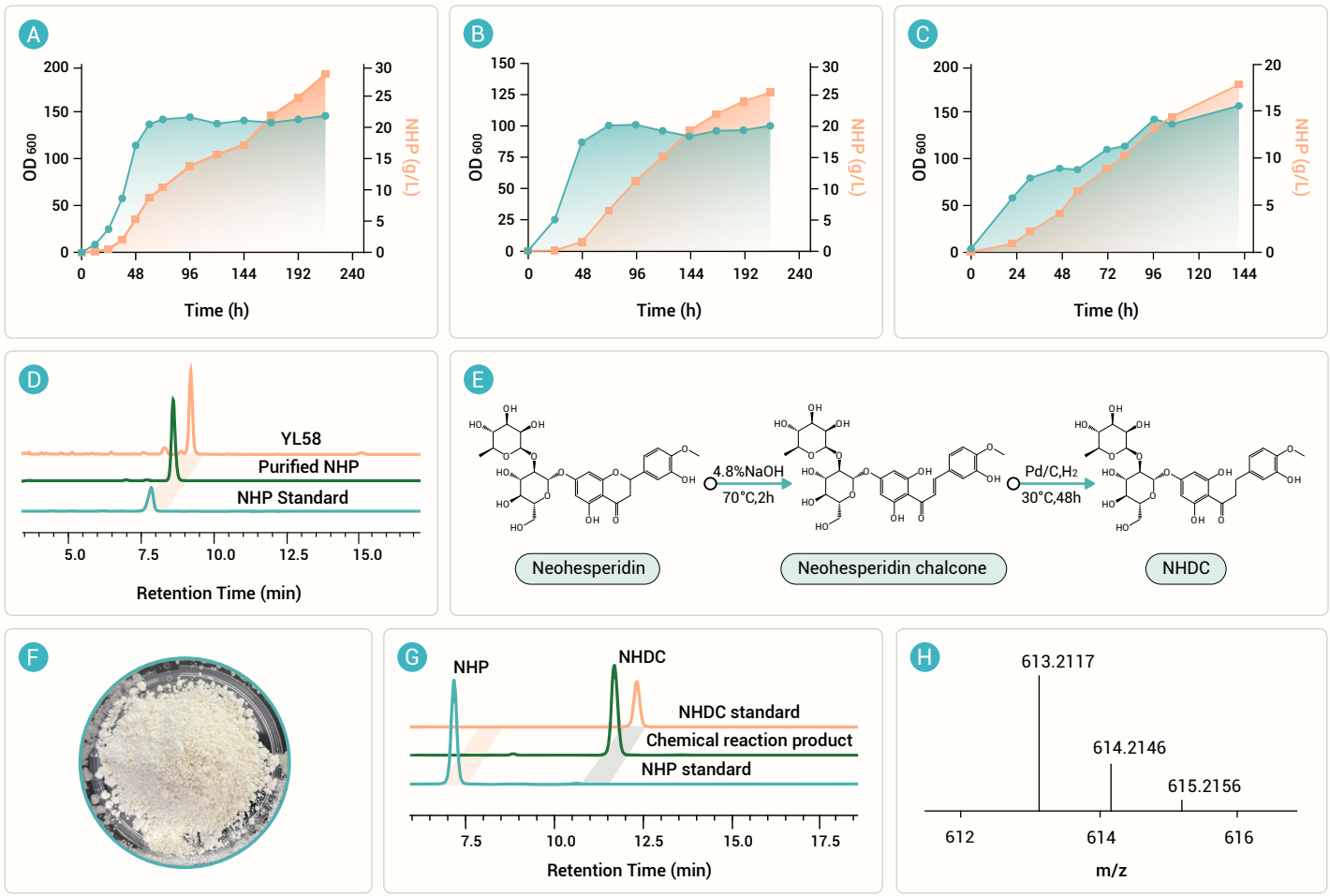

Figure 5. Fed-batch fermentation in 5-L, 200-L and 5000-L bioreactor and chemical synthesis of NHDC (A) The NHP production of the engineering strain YL58 in a 5-L bioreactor. (B) The NHP production of the engineering strain YL58 in a 200-L bioreactor. (C) The NHP production of the engineering strain YL58 in a 5000-L bioreactor. (D) HPLC analysis of the fermented products of the strain YL58 in 200-L bioreactor, purified NHP from fermented product of YL58 and neohesperidin standard. Most impurities were removed. (E) Scheme of NHDC synthesis from NHP. (F) The crude product NHDC obtained from NHP produced by fermentation of engineered strain in this study. (G) HPLC analysis of the NHDC standard, the chemical reaction product of NHP purificated from fermentation broth and NHP standard. (H) MS analysis of crude product NHDC from chemical reaction. All data are presented as mean of n = 3 biologically independent samples and error bars show the standard deviations. Source data are provided as a Supplementary Table.

mulation, we optimized the cofactor supply for the key enzymes *CsF3`H* and *YlOMT*. *OMT* catalyzes the transfer of methyl groups from S-adenosyl-L-methionine (SAM) to substrates, forming *O*-methyl derivatives and S-adenosyl-L-homocysteine (SAH).[51] However, insufficient SAM often obstructs the production of methylation products,[52] and SAH may act as an *OMT* inhibitor.[53] We first added 0.5 g/L methionine during the fermentation process to increase the SAM pool, however, comparing with the control group, the yield of neohesperidin decreased by 20% (Figure S15). Thus, we tried to overexpress SAH hydrolase (*SAHH*) and adenosine kinase (*ADO*) in strain YL52 to enhance SAH degradation and accelerate SAM recycling generating strain YL53[54] and the neohesperidin titer reached 126.32 mg/L (Figure 4D). To further enhance the activity of *CsF3`H* for redirecting naringenin flux toward eirodictyol, we introduced 5-aminolevulinic acid synthase (*ALAS*) to increase the supply of the P450 cofactor heme (Figure S16).[55] This strategy promoted the production of neohesperidin to 192.57 mg/L and effectively reduced naringin accumulation (Figures 4C-D).

Considering the low level of naringenin accumulation, we proposed to further increase the carbon yield by introducing a non-carboxylative malonyl-CoA (NCM) pathway, which could enhance the flux of malonyl-CoA and prevent carbon source loss caused by decarboxylation reaction.[56] When fermenting with 20 g/L glycerol, the neohesperidin titer increased by 17.28% from 117.73 mg/L (YL54) to 138.07 mg/L (YL55), while the naringin titer increased by 19.44% from 150.9 mg/L (YL54) to 180.24 mg/L (YL55), indicating that the malonyl-CoA supply was boosted (Figure 4D). The concomitant significant increase in the yield of the by-product naringin could be attributed to an augmented supply of glycosylation donors, mediated by the heightened availability of carbon precursors. To enhance the channeling of the malonyl-CoA metabolic pool toward target biosynthesis, we strategically amplified the gene dosage of *Eb4CL* and *MdCHS2* through genetic modification. A proportional increase in neohesperidin biosynthesis was observed with incremental amplification of transgene copy numbers. The final strain YL58 achieved a yield of 262.36 mg/L of neohesperidin, while the production of the by-product naringin also showed a slight increase (Figure 4D). Compared with YL55, YL58 exhibited a 26.47% increase in neohesperidin production (from 0.3 mM to 0.43 mM) and a 16.67% increase in naringin production (from 0.24 mM to 0.28 mM) (Figure S17). The above results indicate that carbon flux was further directed towards product synthesis.

Efficient production of neohesperidin in bioreactor and conversion of NHDC

To further enhance neohesperidin production, we conducted fed-batch fermentation of the top-performing engineered strain YL58 in a 5-L bioreactor. To mitigate foam formation and reduce costs, minimal medium (MM) supplemented with glycerol was employed as the carbon source. During the initial 60 h, the OD_{600} surged to 140 and only exhibited minor fluctuations until the end of fermentation (Figure 5A). The enhanced growth of engineered strain YL58 over YL40 was consistent with the hypothesis that product glycosylation alleviates its detrimental effects on yeast cell viability. The producntion of neohesperidin increased rapidly after 24 hours, reaching 28.52 g/L by the end of fermentation (216 h) in the 5-L bioreactor. Finally, 1,352 g glycerol was consumed, achieving a neohesperidin yield of 99.82 g with a glycerol-to-neohesperidin conversion efficiency of 73.83 mg/g, which

is the highest conversion rate of heterologous synthesis of flavonoids so far. To further test our strain under industrial conditions, we employed crude glycerol as the carbon source in a 200-L bioreactor. The strain exhibited performance comparable to that in the 5-L bioreactor, accumulating 25.34 g/L neohesperidin at 216 h (Figure 5B). Notably, the by-product naringin remained relative low level across both 5-L and 200-L fermentations (Figures S18-S19). This suppression might be attributed to the continuous feeding strategy, which maintained glycerol at low concentrations (< 1 g/L) throughout fermentation. Consequently, the limited supply of UDP-glucose from glycerol shifted glycosyltransferase catalytic preference toward neohesperidin synthesis over naringin formation. Subsequently, we performed fermentation in a 5,000-L industrial-scale trial. Fermentation was halted at 130 h due to excessive foam formation to prevent vessel overflow. At the last, the titer of neohesperidin reached 18.55 g/L at 130 h (Figure 5C). Despite the yield reduction, the production rate (142.69 mg/L/h) increased by 8% compared to the 5-L bioreactor. These results demonstrate the strain's robust scalability and significant commercial potential for cost-effective manufacturing of neohesperidin.

Given the efficiency of enzymatic biotransformation from neohesperidin to NHDC is not satisfied industrial production, we employed an alternative chemical conversion strategy according to previous studies.[57] To ensure reaction specificity, neohesperidin was initially purified from fermentation broth, effectively eliminating matrix interference from complex microbial metabolites (Figures 5D & S20). Finally, approximately 50.70 kg neohesperidin was purified from 3100-L fermentation broth, achieving a purity of 98% and an actual yield of 87%. The entire chemical reaction included two critical transformations: (1) cleavage of the C-O bond of neohesperidin to generate neohesperidin chalcone, and (2) following the selective ring-opening reaction of neohesperidin with 4.8% NaOH, the resulting intermediate was subsequently subjected to catalytic hydrogenation using Pt/C as the catalyst and H_2 as the reducing agent, effectively reducing the α, β-unsaturated ketone moiety of neohesperidin chalcone (Figure 5E). Finally, we achieved the synthesis of NHDC from neohesperidin with a conversion rate about 98% (Figures 5F-H).

DISSCUSION AND CONCLUSION

NHDC is an important natural sweetener due to its superior sweetness, low calorie content, safety, and stability.[58,59] Here, we systematically engineered *Y. lipolytica* for *de novo* biosynthesis of neohesperidin by functionally identifying biosynthetic enzymes and optimizing metabolic flux. This study constructed a total of 106 engineering yeasts, including 48 *S. cerevisiae* and 58 *Y. lipolytica*. The final strain comprises 43 chromosomal modifications, including 36 genes integrations and 7 genes deletions (Figure S21). The engineered strain was scaled up from 5-L to 5000-L fermentation tank, achieving the production rate to 0.14 g/L/h. Comparing plant extraction from *Fructus Aurantii*, neohesperidin constitutes approximately 3.8% of the plant's dry weight, producing approximately 1500 kg of dried fruit per acre per year. Through microbial fermentation optimization, our engineered strain generates 1250 kg of neohesperidin annually within a 1 m^3 fermentation system. This industrial-scale output represents a production equivalent to that obtained from traditional cultivation spanning 100,000 m^2.

The identification of key catalytic elements in biosynthetic pathways provides the foundation for the heterologous production of valuable plant natural products.[60] In this study, we screened candidate genes from 25 species across plants, fungi, and bacteria to identify catalytic elements with enhanced activity for neohesperidin pathway reconstruction (Table S7). Notably, we identified a native OMT (*YlOMT*) in *Y. lipolytica* that efficiently catalyzes hesperetin production and the activity is 2.43-fold that of *CsOMT-15* at pH 5.5 (Figure 2C). Previous study showed that *OMTs* might become inactive under acidic conditions in the cytoplasm.[61] Therefore, *YlOMT* is more suitable for producing neohesperidin in *Y. lipolytica*. Furthermore, we have successfully screened *PAL*, *TAL*, *CHS* with higher activities. It is worth noting that these catalytic elements are superior to the enzymes commonly used in flavonoid cell factories at present (Figures 3B-D). Compared to the initial enzyme used, the catalytic activity of *PAL*, *TAL*, and *CHS* has increased 324% (*RgPAL* vs *EbPAL*), 81% (*CluTAL* vs *FjTAL*) and 60% (*MdCHS2* vs *EbCHS*) respectively. Introducing these efficient catalytic components into the construction of engineered strains resulted in a 48-fold increase in naringenin production.

Cofactor balance also plays a crucial role in maintaining intracellular biochemical homeostasis. SAM and heme, as methyl donors for OMTs and cofactors for P450 enzymes, are tightly regulated in microorganisms.[55,62] Exogenous supplementation is expensive and may cause cytotoxicity.[52,54,55] Thus, we accelerated the conversion from SAH to L-homocysteine through the introduction of *SAHH* and *ADO*, increasing the production of neohesperidin by 19.87%. Then we boost cellular heme supply via *ALAS* overexpression. This strategy significantly enhances the activity of *CsF3`H*. The conversion of neohesperidin from naringenin increased by 1.52-fold and the synthesis of the by-product naringin was also reduced (3.68-fold).

Fermenter scale-up cultivation is an effective approach for enhancing the production yield of microbial cell factories.[21] In this study, we successfully increased the production of neohesperidin by more than 100-fold through continuous fed-batch scale-up cultivation. First, during the 5-L scale-up cultivation, the continuous feeding increased the fermentation carbon source around 20-fold compared to shake flask cultivation. Second, the supplementation of a large amount of carbon source increased the cell population by more than approximately 10-fold compared to shake flask cultivation. Finally, by controlling the continuous feeding process, the proportion of by-products was also significantly reduced. For example, the proportion of the byproduct naringin decreased by 26.72% (5-L fermenter, from 38.31% to 11.59%) and 29.13% (200-L fermenter, from 38.31% to 9.18%), respectively. These factors together contributed to a significant increase in neohesperidin production. This feeding strategy is also applicable to the fermentation of other compounds prone to glycosylation byproduct formation. Excessive foam formation is a factor that compromises the efficiency of aerobic fermentation processes. Subsequently, the composition of the culture medium will be optimized and alternative antifoaming agents will be evaluated to mitigate foam formation during fermentation.

In conclusion, this study combined engineered microbial production of neohesperidin with chemical catalysis to obtain NHDC, thereby enabling the sustainable and efficient synthesis of this low-calorie sweetener. The coupling strategy exhibits promising applicability in industrial manufacturing contexts. Using crude glycerol as a carbon source also enables high-level neohesperidin production, significantly enhancing the economic feasibility of this technology. The implementation of diverse metabolic and fermentation engineering strategies has established a robust platform for producing various flavonoid derivatives. As a natural low-calorie sweetener with various biological activities, NHDC not only has the potential to alleviate diseases such as diabetes but also holds broad prospects for future applications in nutrition regulation and related fields.

REFERENCES

1. Suez J., Korem T., Zeevi D., et al. (2014). Artificial sweeteners induce glucose intolerance by altering the gut microbiota. *Nature* **514**:181–186. DOI:10.1038/nature13793
2. Zani F., Blagih J., Gruber T., et al. (2023). The dietary sweetener sucralose is a negative modulator of T cell-mediated responses. *Nature* **615**:705–711. DOI:10.1038/s41586-023-05801-6
3. Schiffman S. S., Scholl E. H., Furey T. S., et al. (2023). Toxicological and pharmacokinetic properties of sucralose-6-acetate and its parent sucralose: *in vitro* screening assays. *J. Toxicol. Env. Heal. B.* **26**:307–341. DOI:10.1080/10937404.2023.2213903
4. Shi Z., Lei H., Chen G., et al. (2021). Impaired intestinal *Akkermansia muciniphila*and aryl hydrocarbon receptor ligands contribute to nonalcoholic fatty liver disease in mice. *Msystems* **6**:1-17. e00985-20,DOI:10.1128/mSystems.00985-20
5. Xue Q., Su X., Yu W., et al. (2024). Efficient production of neohesperidin enabled by protein engineering of rhamnosyltransferase Cm1,2RhaT. *ACS Sustainable Chem. Eng.* **12**:1960–1972. DOI:10.1021/acssuschemeng.3c06262
6. Horowitz R. M. and Gentili B. (1969). Taste and structure in phenolic glycosides. *J. Agric. Food Chem.* **17**:696–700. DOI:10.1021/jf60164a049
7. Shi Q., Song X., Fu J. L., et al. (2015). Artificial sweetener neohesperidin dihydrochalcone showed antioxidative, anti-inflammatory and anti-apoptosis effects against paraquat-induced liver injury in mice. *Int. Immunopharmacol.* **29**:722–729. DOI:10.1016/j.intimp.2015.09.003
8. Baêr A., Borrego F., Benavente O., et al. (1990). Neohesperidin dihydrochalcone: Properties and applications. *Astron. Astrophys.* **23**:371–376. DOI:10.1086/116898
9. Huang J., Lu Y.-J., Guo C., et al. (2021). The study of citrus-derived flavonoids as

effective bitter taste inhibitors. *J. Sci. Food Agric.* **101**:5163–5171. DOI:10.1002/jsfa.11162
10. Lindley M. G., Beyts P. K., Canales I., et al. (1993). Flavor modifying characteristics of the intense sweetener neohesperidin dihydrochalcone. *J. Food Sci.* **58**:592–594. DOI:10.1111/j.1365-2621.1993.tb04331.x
11. Xiao Y., Fu F., Wei Y., et al. (2022). Online extraction-DPPH-HPLC-DAD-QTOF-MS system for efficient screening and identification of antioxidants from *Citrus aurantium* L. *var. amara (Rutaceae): Integrating sample preparation and antioxidants profiling. Antioxidants* **11**:1–12. DOI:10.3390/antiox11051014
12. Sun Y., Tao W., Huang H., et al. (2019). Flavonoids, phenolic acids, carotenoids and antioxidant activity of fresh eating citrus fruits, using the coupled *in vitro* digestion and human intestinal HepG2 cells model. *Food. Chem.* **279**:321–327. DOI:10.1016/j.foodchem.2018.12.019
13. Winkel-Shirley B. (2001). Flavonoid biosynthesis. *A colorful model for genetics, biochemistry, cell biology, and biotechnology. Plant Physiol.* **126**:485–493. DOI:10.1104/pp.126.2.485
14. Zhu S., Wu J., Du G., et al. (2014). Efficient synthesis of eriodictyol from L-tyrosine in *Escherichia coli. Appl. Environ. Microb.* **80**:3072–3080. DOI:10.1128/aem.03986-13
15. Frydman A., Liberman R., Huhman D. V., et al. (2013). The molecular and enzymatic basis of bitter/non-bitter flavor of citrus fruit: Evolution of branch-forming rhamnosyltransferases under domestication. *Plant J.* **73**:166–178. DOI:10.1111/tpj.12030
16. Ru Z., Liu M., Chen Q., et al. (2025). High-level *de novo* production of (2*S*)-naringenin in *Yarrowia lipolytica* using metabolic and enzyme engineering. *ACS Agric. Sci. Technol.* **5**:784–793. DOI:10.1021/acsagscitech.4c00729
17. Wang Y. Y., Huang R. Q., Gao S., et al. (2025). Identification of two new flavone 4`-*O*-methyltransferases and their application in *de novo* biosynthesis of (2*S*)-hesperetin in *Yarrowia lipolytica. Synth. Syst. Biotechnol.* **10**:728–736. DOI:10.1016/j.synbio.2025.03.003
18. Liu J., Xiao Z., Zhang S., et al. (2023). Restricting promiscuity of plant flavonoid 3`-hydroxylase and 4`-*O*-methyltransferase improves the biosynthesis of (2*S*)-hesperetin in *E. coli. J. Agric. Food Chem.* **71**:9826–9835. DOI:10.1021/acs.jafc.3c02071
19. Groenewald M., Boekhout T., Neuveglise C., et al. (2014). *Yarrowia lipolytica*: Safety assessment of an oleaginous yeast with a great industrial potential. *Crit. Rev. Microbiol.* **40**:187–206. DOI:10.3109/1040841x.2013.770386
20. Yue M., Liu M., Gao S., et al. (2024). High-level *de novo* production of (2*S*)-eriodictyol in *Yarrowia Lipolytica* by metabolic pathway and NADPH regeneration engineering. *J. Agric. Food Chem.* **72**:4292–4300. DOI:10.1021/acs.jafc.3c08861
21. Chen B., Liu X., Wang Y., et al. (2023). Production of the antidepressant orcinol glucoside in *Yarrowia lipolytica* with yields over 6,400-fold higher than plant extraction. *PLoS Biol.* **21**:1–15. DOI:10.1371/journal.pbio.3002131
22. Wang Y. A., Liu X. A., Chen B. H., et al. (2022). Metabolic engineering of *Yarrowia lipolytica* for scutellarin production. *Synth. Syst. Biotechnol.* **7**:958–964. DOI:10.1016/j.synbio.2022.05.009
23. Jensen N. B., Strucko T., Kildegaard K. R., et al. (2014). EasyClone: Method for iterative chromosomal integration of multiple genes in *Saccharomyces cerevisiae. FEMS Yeast Res.* **14**:238–248. DOI:10.1111/1567-1364.12118
24. Liu X., Cheng J., Zhang G., et al. (2018). Engineering yeast for the production of breviscapine by genomic analysis and synthetic biology approaches. *Nat. Commun.* **9**:1–10. DOI:10.1038/s41467-018-02883-z
25. Schlangen K., Miosic S., Thill J., et al. (2010). Cloning, functional expression, and characterization of a chalcone 3-hydroxylase from *Cosmos sulphureus. J. Exp. Bot.* **61**:3451–3459. DOI:10.1093/jxb/erq169
26. Liu X., Gong Q., Zhao C., et al. (2023). Genome-wide analysis of cytochrome P450 genes in *Citrus clementina* and characterization of a CYP gene encoding flavonoid 3`-hydroxylase. *Hortic. Res.* **10**:1–14. DOI:10.1093/hr/uhac283
27. Seitz C., Eder C., Deiml B., et al. (2006). Cloning, functional identification and sequence analysis of flavonoid 3`-hydroxylase and flavonoid 3`,5`-hydroxylase cDNAs reveals independent evolution of flavonoid 3`,5`-hydroxylase in the Asteraceae family. *Plant Mol. Biol.* **61**:365–381. DOI:10.1007/s11103-006-0012-0
28. Gao S., Xu X., Zeng W., et al. (2020). Efficient biosynthesis of (2*S*)-eriodictyol from (2*S*)-naringenin in *Saccharomyces cerevisiae* through a combination of promoter adjustment and directed evolution. *ACS. Synth. Biol.* **9**:3288–3297. DOI:10.1021/acssynbio.0c00346
29. Zhou J.-M., Gold N. D., Martin V. J. J., et al. (2006). Sequential *O*-methylation of tricetin by a single gene product in wheat. *Biochim. Biophys. Acta. Gen. Subj.* **1760**:1115–1124. DOI:10.1016/j.bbagen.2006.02.008
30. Wils C. R., Brandt W., Manke K., et al. (2013). A single amino acid determines position specificity of an *Arabidopsis thaliana* CCoAOMT-like *O*-methyltransferase. *FEBS Lett.* **587**:683–689. DOI:10.1016/j.febslet.2013.01.040
31. Schröder G., Wehinger E., Lukacin R., et al. (2004). Flavonoid methylation: A novel 4`-*O*-methyltransferase from *Catharanthus roseus*, and evidence that partially methylated flavanones are substrates of four different flavonoid dioxygenases. *Phytochemistry* **65**:1085–1094. DOI:10.1016/j.phytochem.2004.02.010
32. Berim A., Hyatt D. C. and Gang D. R. (2012). A set of regioselective *O*-methyltransferases gives rise to the complex pattern of methoxylated flavones in sweet basil. *Plant Physiol.* **160**:1052–1069. DOI:10.1104/pp.112.204164
33. Noguchi A., Horikawa M., Fukui Y., et al. (2009). Local differentiation of sugar donor specificity of flavonoid glycosyltransferase in Lamiales. *Plant Cell* **21**:1556–1572. DOI:10.1105/tpc.108.063826
34. Cao M., Gao M., Suastegui M., et al. (2020). Building microbial factories for the production of aromatic amino acid pathway derivatives: From commodity chemicals to plant-sourced natural products. *Metab. Eng.* **58**:94–132. DOI:10.1016/j.ymben.2019.08.008
35. Yahyaa M., Davidovich-Rikanati R., Eyal Y., et al. (2016). Identification and characterization of UDP-glucose: Phloretin 4`-*O*-glycosyltransferase from *Malus* x *domestica* Borkh. *Phytochemistry* **130**:47–55. DOI:10.1016/j.phytochem.2016.06.004
36. Liu T., Liu Y., Li L., et al. (2021). *De novo* biosynthesis of polydatin in *Saccharomyces cerevisiae. J. Agric. Food Chem.* **69**:5917–5925. DOI:10.1021/acs.jafc.1c01557
37. Martinez-Munoz G. A. and Kane P. (2008). Vacuolar and plasma membrane proton pumps collaborate to achieve cytosolic pH homeostasis in yeast. *J. Biol. Chem.* **283**:20309–20319. DOI:10.1074/jbc.M710470200
38. Pandey R. P., Parajuli P., Koffas M. A. G., et al. (2016). Microbial production of natural and non-natural flavonoids: Pathway engineering, directed evolution and systems/synthetic biology. *Biotechnol. Adv.* **34**:634–662. DOI:10.1016/j.biotechadv.2016.02.012
39. Lv Y., Marsafari M., Koffas M., et al. (2019). Optimizing oleaginous yeast cell factories for flavonoids and hydroxylated flavonoids biosynthesis. *ACS Synth. Biol.* **8**:2514–2523. DOI:10.1021/acssynbio.9b00193
40. Saez-Saez J., Wang G., Marella E. R., et al. (2020). Engineering the oleaginous yeast *Yarrowia lipolytica* for high-level resveratrol production. *Metab. Eng.* **62**:51–61. DOI:10.1016/j.ymben.2020.08.009
41. Koopman F., Beekwilder J., Crimi B., et al. (2012). *De novo* production of the flavonoid naringenin in engineered *Saccharomyces cerevisiae. Microb. Cell Fact.* **11**:1-15. 155,DOI:10.1186/1475-2859-11-155
42. Shen Y., Li X., Chai T., et al. (2016). Outer-sphere residues influence the catalytic activity of a chalcone synthase from *Polygonum cuspidatum. FEBS Open Bio.* **6**:610–618. DOI:10.1002/2211-5463.12072
43. Liu B. Y., Falkenstein-Paul H., Schmidt W., et al. (2003). Benzophenone synthase and chalcone synthase from *Hypericum androsaemum* cell cultures: cDNA cloning, functional expression, and site-directed mutagenesis of two polyketide synthases. *Plant J.* **34**:847–855. DOI:10.1046/j.1365-313X.2003.01771.x
44. Waki T., Mameda R., Nakano T., et al. (2020). A conserved strategy of chalcone isomerase-like protein to rectify promiscuous chalcone synthase specificity. *Nat. Commun.* **11**:1–14. DOI:10.1038/s41467-020-14558-9
45. Pandith S. A., Ramazan S., Khan M. I., et al. (2020). Chalcone synthases (CHSs): The symbolic type III polyketide synthases. *Planta* **251**:1–29. DOI:10.1007/s00425-019-03307-y
46. Jez J. M., Bowman M. E. and Noel J. P. (2002). Expanding the biosynthetic repertoire of plant type III polyketide synthases by altering starter molecule specificity. *Proc. Natl. Acad. Sci. USA* **99**:5319–5324. DOI:10.1073/pnas.082590499
47. Hwang H. G., Milito A., Yang J.-S., et al. (2023). Riboswitch-guided chalcone synthase engineering and metabolic flux optimization for enhanced production of flavonoids. *Metab. Eng.* **75**:143–152. DOI:10.1016/j.ymben.2022.12.006
48. Konzock O., Tous-Mohedano M., Cibin I., et al. (2023). Cinnamic acid and *p*-coumaric acid are metabolized to 4-hydroxybenzoic acid by *Yarrowia lipolytica. AMB Express* **13**:1–10. DOI:10.1186/s13568-023-01590-3
49. Li H., Ma W., Lyv Y., et al. (2022). Glycosylation modification enhances (2*S*)-naringenin production in *Saccharomyces cerevisiae. ACS Synth. Biol.* **11**:2339–2347. DOI:10.1021/acssynbio.2c00065
50. Wei Y. F., Ang E. L. and Zhao H. M. (2018). Recent developments in the application of P450 based biocatalysts. *Curr. Opin. Chem. Biol.* **43**:1–7. DOI:10.1016/j.cbpa.2017.08.006
51. Ye C. and Tu B. P. (2018). Sink into the epigenome: Histones as repositories that influence cellular metabolism. *Trends Endocrinol. Metab.* **29**:626–637. DOI:10.1016/j.tem.2018.06.002
52. Zhou Z., Zhang X., Wu J., et al. (2022). Targeting cofactors regeneration in methylation and hydroxylation for high level production of Ferulic acid. *Metab. Eng.* **73**:247–255. DOI:10.1016/j.ymben.2022.08.007
53. Hoffman D. R., Haning J. A. and Cornatzer W. E. (1981). Microsomal phosphatidylethanolamine methyltransferase: Inhibition by S-adenosylhomocysteine. *Lipids* **16**:561–567. DOI:10.1007/bf02534900
54. Chen R. B., Gao J. Q., Yu W., et al. (2022). Engineering cofactor supply and recycling to drive phenolic acid biosynthesis in yeast. *Nat. Chem. Biol.* **18**:520–529. DOI:10.1038/s41589-022-01014-6
55. Yu F., Zhao X., Zhou J., et al. (2023). Biosynthesis of high-active hemoproteins by the efficient heme-supply *Pichia Pastoris* chassis. *Adv. Sci.* **10**:1–14. DOI:10.1002/advs.202302826
56. Li J., Mu X., Dong W., et al. (2024). A non-carboxylative route for the efficient synthesis of central metabolite malonyl-CoA and its derived products. *Nat. Catal.* **7**:361–374. DOI:10.1038/s41929-023-01103-2
57. Zou Y., Li X., Xin X., et al. (2024). Microbial-driven synthesis and hydrolysis of neohesperidin dihydrochalcone: Biotransformation process and feasibility investigation. *J. Agric. Food Chem.* **72**:4246–4256. DOI:10.1021/acs.jafc.3c08339

58. Ruiz-Ojeda F. J., Plaza-Díaz J., Sáez-Lara M. J., et al. (2019). Effects of sweeteners on the gut microbiota: A review of experimental studies and clinical trials. *Adv. Nutr.* **10**:31–48. DOI:10.1093/advances/nmy037
59. Younes M., Aquilina G., Castle L., et al. (2022). Re-evaluation of neohesperidine dihydrochalcone (E 959) as a food additive. *EFSA J.* **20**:1–81. DOI:10.2903/j.efsa.2022.7595
60. Zhu X., Liu X., Liu T., et al. (2021). Synthetic biology of plant natural products: From pathway elucidation to engineered biosynthesis in plant cells. *Plant Commun.* **2**:1-16. 100229,DOI:10.1016/j.xplc.2021.100229
61. Wang P., Li C., Li X., et al. (2021). Complete biosynthesis of the potential medicine icaritin by engineered *Saccharomyces cerevisiae* and *Escherichia coli*. *Sci. Bull.* **66**:1906–1916. DOI:10.1016/j.scib.2021.03.002
62. Thomas D. and SurdinKerjan Y. (1997). Metabolism of sulfur amino acids in *Saccharomyces cerevisiae*. *Microbiol. Mol. Biol. R.* **61**:503–532. DOI:10.1128/.61.4.503-532.1997

FUNDING AND ACKNOWLEDGMENTS

This work was supported by the National Key R&D Program of China (Grant No. 2023YFC3503903), the Joint Fund Projects of the National Natural Science Foundation of China (U23A20219) and Tianjin Synthetic Biotechnology Innovation Capacity Improvement Project (TSBICIP-IJCP-002). The funders had no role in study design, data collection and analysis, decision to publish, or preparation of the manuscript.

AUTHOR CONTRIBUTIONS

H.J, X.Z and W.L conceived, designed and drafted the manuscript. X.Z and W.L performed experiments. H.J, X.Z, W.L and X.L analyzed data. H.C and J.C analyzed the structure and mechanism of OMT. J.L, N.A and L.S conducted relevant experiments. Y.L and X.Z conducted chemical synthesis of NHDC. All authors read and approved the final manuscript.

DECLARATION OF INTERESTS

The authors declare no competing interests.

ETHICAL STATEMENT AND PATIENT CONSENT

Not applicable.

DATA AND CODE AVAILABILITY

Data generated or analyzed during this study are included in the published article and its Supplemental information. Any additional data are available from the corresponding author upon reasonable request.

SUPPLEMENTAL INFORMATION

It can be found online at https://doi.org/10.59717/j.xinn-life.2026.100190